

# Entangling four logical qubits beyond break-even in a nonlocal code

Yifan Hong,<sup>1,\*</sup> Elijah Durso-Sabina,<sup>2</sup> David Hayes,<sup>2</sup> and Andrew Lucas<sup>1</sup>

<sup>1</sup>*Department of Physics and Center for Theory of Quantum Matter,  
University of Colorado, Boulder, CO 80309, USA*

<sup>2</sup>*Quantinuum, Broomfield, CO 80021, USA*

(Dated: June 6, 2024)

Quantum error correction protects logical quantum information against environmental decoherence by encoding logical qubits into entangled states of physical qubits. One of the most important near-term challenges in building a scalable quantum computer is to reach the break-even point, where logical quantum circuits on error-corrected qubits achieve higher fidelity than equivalent circuits on uncorrected physical qubits. Using Quantinuum’s H2 trapped-ion quantum processor, we encode the GHZ state in four logical qubits with fidelity  $99.5 \pm 0.15\% \leq F \leq 99.7 \pm 0.1\%$  (after postselecting on over 98% of outcomes). Using the same quantum processor, we can prepare an uncorrected GHZ state on four physical qubits with fidelity  $97.8 \pm 0.2\% \leq F \leq 98.7 \pm 0.2\%$ . The logical qubits are encoded in a  $[[25, 4, 3]]$  Tanner-transformed long-range-enhanced surface code. Logical entangling gates are implemented using simple swap operations. Our results are a first step towards realizing fault-tolerant quantum computation with logical qubits encoded in geometrically nonlocal quantum low-density parity check codes.

*Introduction.*— It is widely believed that fault tolerance will be necessary for quantum computers to outperform classical computers on large-scale problems. Decoherence, if left ignored, will eventually destroy entanglement and any quantum advantage in computation. A critical milestone for the development of a quantum computer will, therefore, be the protection of logical qubits and the implementation of logical gates whose error rates are below that of physical qubits and circuits which are not error-corrected. When logical qubits are more robust than physical qubits, we have reached *break-even*.

Since the discovery of topological quantum codes [1, 2] and their promise to preserve quantum information for arbitrarily long times with a relatively high tolerance for errors [3, 4], there have been immense efforts to implement such codes in current architectures [5–9]. Unfortunately, the resource requirements for large-scale, fault-tolerant quantum computation using topological codes with current hardware specifications may be enormous [10].

More generally, it is known that these overheads cannot be substantially improved in planar architectures (codes) with only nearest-neighbor connectivity [11]. To avoid this fundamental challenge, quantum low-density parity-check (LDPC) codes [12–19] have been developed to significantly reduce the resource overheads for error correction [20, 21]. To avoid the constraints of Ref. [11], these codes will necessarily require long-range connectivity [22, 23]. Platforms with such capabilities may be able to significantly reduce the overhead for quantum error correction, and a number of recent proposals have been made for how to incorporate limited long-range connectivity into hardware [24–27] to ameliorate the constraints of spatial locality.

Thus far, we are not aware of any explicit implementation of a nonlocal LDPC code in any quantum hardware. Other recent demonstrations of break-even operations we are aware of include the use of a small 7-qubit Steane code [8, 28] and the use of concatenated error detection codes [9], neither of which achieve the high-encoding rates of qLDPC codes. While such codes may improve performance, to truly avoid large resource overheads in a scalable way, it is crucial to use a nonlocal code which protects logical qubits in a more complex manner, yet which is also amenable to quantum hardware.

This work provides a proof-of-principle demonstration that nonlocal codes can improve the performance of present-day quantum computers. We have implemented a  $[[25, 4, 3]]$  quantum LDPC code (encoding 4 logical qubits in 25 physical qubits, with the smallest logical operator acting on 3 physical qubits) on Quantinuum’s H2 trapped-ion quantum computer [29], which was configured with 32 physical qubits at the time of the experiments. This encoding enables us to prepare an error-corrected, logical 4-qubit entangled GHZ state beyond the break-even point, with mild postselection overhead, for the first time. Using the existing hardware, it would not have been possible to attempt such a demonstration, even in principle, by using four surface code patches (with 36 total physical) to encode the logical qubits. This work highlights the importance of choosing good hardware-suited codes with efficient logical gates. The long-range-enhanced surface code [26] underlying our methods will be scalable to larger trapped-ion QCCD processors [30–33] as well as to neutral atom arrays [8, 34–37] for the foreseeable future.

*Quantum encoding.*— The quantum LDPC code we use is a Calderbank-Shor-Steane (CSS) stabilizer code [38–40], which is defined by a stabilizer group of Pauli strings that mutually commute and act trivially on logical codewords. In a CSS code, these Pauli strings are generated by products of strictly  $X$  or  $Z$  operators act-

\* yifan.hong@colorado.edu

ing on  $n$  qubits. Given the Pauli (anti)commutation relations, it is helpful to organize data about the stabilizer group in a pair of matrices  $H_{X,Z}$  with  $\mathbb{F}_2 = \{0, 1\}$  coefficients. Each row of the matrix  $H_X$ , which in turn has  $n$  columns, fixes one of the stabilizers of the code to be a product of Pauli  $X$ s on all qubits with a 1 in the corresponding column;  $H_Z$  is defined similarly. To be a valid code, we require  $X$  and  $Z$  stabilizers to commute, which means  $H_X H_Z^T = 0$  (here multiplication/addition are mod 2).

A convenient way to build a quantum code is the hypergraph product [13] of a classical linear code with itself. For an input  $m \times n$  classical parity-check matrix  $H$ , the resulting CSS stabilizer matrices take the form

$$H_X = (H \otimes \mathbf{1}_n \mid \mathbf{1}_m \otimes H^T) \quad (1a)$$

$$H_Z = (\mathbf{1}_n \otimes H \mid H^T \otimes \mathbf{1}_m). \quad (1b)$$

If the classical input code has parameters  $[n, k, d]$  with  $m = n - k$  parity checks (meaning that there are  $n$  classical bits encoding  $k$  logicals, with code distance  $d$ ), then so long as the classical code has no redundant parity checks, the resulting quantum CSS hypergraph product code has parameters  $[[n^2 + (n - k)^2, k^2, d]]$ . The geometrical layout of the quantum code can be understood as a Cartesian graph product between those of its classical input codes. While the hypergraph product can produce codes with constant rate ( $k \propto n$ ), the distance scaling is sublinear ( $d \lesssim \sqrt{n}$ ). Nonetheless, this distance is preserved under standard syndrome extraction techniques with circuit-level noise [41], a feature not supported by other quantum codes such as the Steane code [40].

We now summarize the construction of our quantum LDPC code, with a graphical depiction in Fig. 1. For the classical input code, we first pick a  $[3, 2, 2]$  parity code consisting of a single, global parity check on all three physical bits. We then concatenate two of the physical bits with a  $[2, 1, 2]$  repetition code to obtain a  $[5, 2, 3]$  code. We then take the hypergraph product of this  $[5, 2, 3]$  code with itself to obtain a  $[[34, 4, 3]]$  CSS code. Finally, we perform a quantum Tanner transformation [19] to reduce the number of physical qubits from 34 to 25, while preserving both  $k$  and  $d$ . We note that the quantum Tanner transformation does not preserve the generic circuit-level distance property mentioned earlier; however, we can still mitigate the effects of correlated errors by choosing a clever pattern for syndrome extraction like that for the rotated surface code [42]. The order of CNOTs is carefully chosen so that all correlated ancilla (hook) errors end up “against the grain” of the logical operators, and so  $d = 3$  errors on the ancilla qubits are necessary to affect the codespace. This code is a minimal example of a more general family of long-range-enhanced surface codes [26], which possess the fewest nonlocal stabilizers necessary to avoid the constraints of locality [11], while adding  $O(1)$  logical qubits.

The standard protocol to prepare the GHZ state on 4 qubits is to initialize the qubits in  $|+000\rangle$  and then apply

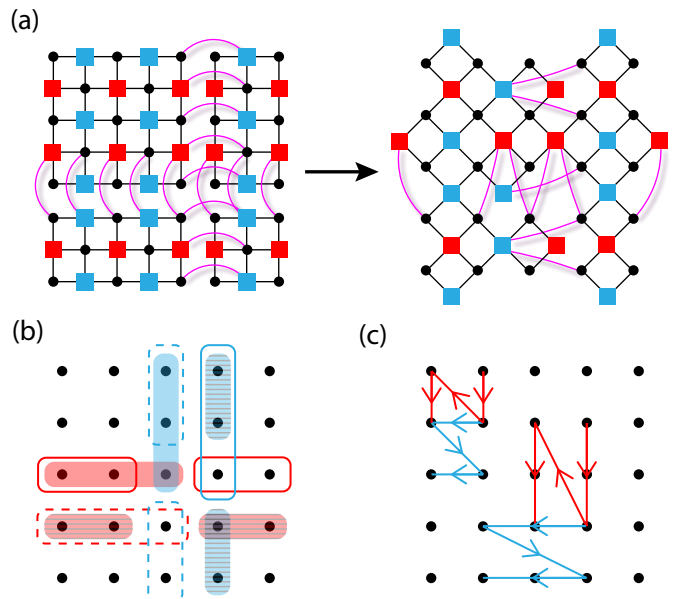


FIG. 1. The code construction is illustrated. Circles and red (blue) squares denote qubits and  $X$  ( $Z$ )-type stabilizers respectively, with edges representing their connectivity. Magenta lines denote long-range interactions. (a) A quantum Tanner transformation reduces the number of physical qubits from 34 to 25. (b) The support of the logical  $X$  and  $Z$  operators for logical qubits 1-4 are drawn with shaded boxes, solid lines, dashed lines, and striped boxes respectively. (c) The order of CNOT gates for distance-preserving syndrome extraction is depicted for a selection of stabilizers.

CNOTs between the  $|+\rangle$  qubit (control) and the rest (target); here  $Z|0\rangle = |0\rangle$  and  $X|+\rangle = |+\rangle$ . Since our code is CSS and has a distance-preserving syndrome extraction circuit, we can perform a transversal initialization into the logical  $|\bar{0}\bar{0}\bar{0}\bar{0}\rangle$  state by initializing all physical qubits in  $|0\rangle^{\otimes n}$  and then measuring all  $X$ -type stabilizers. The stabilizer measurement can be performed by initializing ancillas in the  $|+\rangle$  state, performing CNOT gates between the ancillas (control) and physical qubits (target) according to the pattern in Fig. 1c, and finally measuring all ancillas in the  $X$  basis. We then prepare the third logical qubit in the  $|+\bar{\rangle}$  state by measuring one of its logical  $\bar{X}_3$  operators three times and postselecting on the agreement of all three outcomes in order to mitigate the effects of readout error. After postselection, a logical  $\bar{Z}_3$  is then applied (offline) if the agreed outcome is  $-1$ . After preparing the logical  $|\bar{0}\bar{0}\bar{+}\bar{0}\rangle$  state, we perform the desired logical CNOT gates by permuting the data qubits – a feature inherited from the  $[3, 2, 2]$  parity code. This relabeling step can be done in software in our particular experiment. In particular, two combinations of “fold-swaps” are sufficient: see Fig. 2. Finally, we perform a transversal measurement of all logical qubits in either the  $X$  or  $Z$  basis by measuring all physical qubits in that basis. This transversal measurement is then used to reconstruct a final syndrome which is not subject to

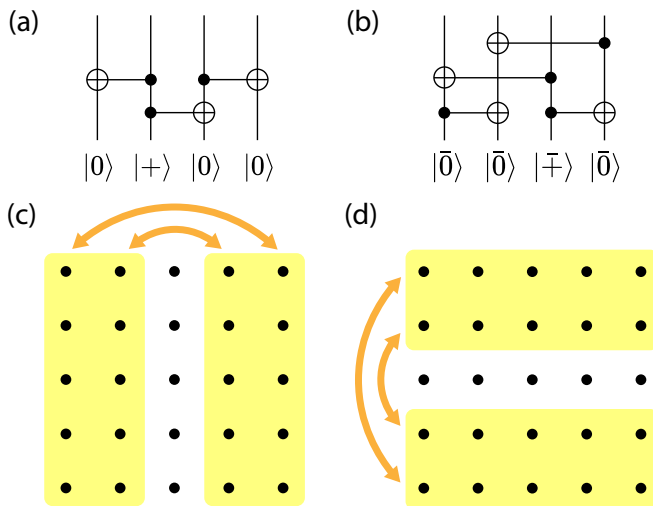


FIG. 2. The procedures for preparing the physical and logical 4-qubit GHZ states are illustrated. (a) The quantum circuit which prepares the physical GHZ state. (b) The circuit which prepares the logical GHZ state. (c-d) A combination of fold swaps implements the above logical circuit while preserving the stabilizer group.

circuit-level noise and can be used to correct errors. All error correction is performed “in software” by tracking the Pauli frame: the final logical measurement outcomes are modified according to a decoding algorithm. We use belief-propagation with ordered statistics decoding (BP+OSD) [43, 44], specifically the “minimum-sum” (10 iterations) and “combination sweep” ( $\lambda = 14$ ) strategies of BP and OS respectively, to infer physical errors based on the syndrome measurement outcomes.

We now discuss the fault tolerance (or lack thereof) of each of the aforementioned steps in our logical GHZ protocol. As previously shown, our syndrome extraction circuit is distance-preserving and so we do not need to worry about ancilla hook errors. However, since we only perform a single round of syndrome extraction, one may worry about the effects of ancilla measurement errors. For example, in a large surface code, a single flipped check in the middle of the code may cause a matching decoder to pair it to the boundary, resulting in a large error string. Fortunately, for our distance three code, any single flipped  $X$ -check can be caused by a single-qubit  $Z$  error, and so we do not suffer from this type of error propagation. For the logical  $\bar{X}_3$  measurement, a single  $Z$  error on a physical qubit prior to the measurements can spoil the result, and so this step is not fault tolerant. We note that a fault-tolerant procedure of measuring  $\bar{X}_3$  can be done using generalized lattice surgery techniques [45], though this would add considerable overhead (and requires more physical qubits than were available in H2 at the time) and so we leave it to future work. The physical qubit permutations to implement the fold-swaps can be achieved by a simple relabeling in software and so is fault tolerant by definition. Lastly, the final measure-

GHZ experiment	$\bar{z}$ mismatch (%)	$\bar{x}$ mismatch (%)
Physical	$1.3 \pm 0.2$	$0.9 \pm 0.1$
Logical (No QEC)	$5.7 \pm 0.5$	$2.9 \pm 0.3$
Logical (with QEC)	$0.3 \pm 0.1$	$0.2 \pm 0.1$

TABLE 1. Fidelity of GHZ state preparation in experiment. The second column displays the percentage of runs when the four  $Z$  measurement outcomes disagreed. The third column displays the percentage of runs when the product of the four  $X$  measurements was  $-1$ . Standard errors for the data are also shown.

ment of all physical qubits is transversal and so is also fault tolerant.

*Experimental results.*— The experiments described in this work used the H2 trapped-ion processor described in Ref. [29]. The H2 processor was configured with 32 trapped-ion qubits, all of which can be directly gated with each other using ion-transport operations to pair any two-qubits in a single potential well — a crucial feature for our  $[[25, 4, 3]]$  code. Physical-level entangling operations are implemented using a Mølmer-Sørensen interaction [46] driven by lasers directed to the four gating regions. Likewise, physical level single-qubit gates, reset, and measurement all take place in these same regions using additional lasers systems. At the time of these experiments, the typical error rates in H2 were as follows:  $< 2 \times 10^{-3}$  two-qubit gate error,  $\approx 3 \times 10^{-5}$  single-qubit gate error, and  $\approx 2 \times 10^{-3}$  state preparation and measurement (SPAM) error.

For the physical GHZ experiment, we run the circuit in Fig. 2a for 10,000 shots, measuring all physical qubits in the  $Z$  basis for 5000 shots and in the  $X$  basis for the other half. For the logical GHZ experiment, we run the circuit in Fig. 2b for 5000 shots, with 2500 shots each dedicated to logical  $\bar{X}$  and  $\bar{Z}$  readout. Uncertainties in the data are computed using the standard error  $\sigma = \sqrt{p(1-p)/N}$ , where  $N$  is the number of shots. For a perfect GHZ state, we expect all  $Z$  measurement outcomes to agree and the product of all  $X$  measurement outcomes to have even parity. The mismatch rates in the experimental data from these theoretical predictions are tabulated in Table 1. In addition to the error-corrected logical results, we also give the uncorrected logical results which are obtained by simply ignoring the syndrome values (i.e. no feedback).

Since the GHZ state is a stabilizer state with generators  $\{Z_1Z_2, Z_2Z_3, Z_3Z_4, X_1X_2X_3X_4\}$ , we can compute simple upper and lower bounds on the GHZ fidelity of our experimental state  $\rho$ . Because  $|\text{GHZ}\rangle$  is a pure state, the fidelity [47] takes the form

$$F_{\text{GHZ}}(\rho) = \langle \text{GHZ} | \rho | \text{GHZ} \rangle \equiv \langle \rho \rangle_{\text{GHZ}}. \quad (2)$$

We now compute an upper bound for the experimental fidelities. First, notice that the two projectors  $P_z^\pm$  onto whether the  $Z$  measurement outcomes agree ( $P_z^+ = (1 + Z_1Z_2)(1 + Z_2Z_3)(1 + Z_3Z_4)/8$ ) or disagree ( $P_z^- = 1 - P_z^+$ )

form a projection-valued measure that splits the Hilbert space into two orthogonal subspaces. Using the fact that  $\langle P_z^+ \rangle_{\text{GHZ}} = 1$ , i.e. the GHZ state strictly lives in the  $P_z^+$  subspace, we can upper bound the fidelity (2) by

$$F_{\text{GHZ}}(\rho) \leq \text{tr}(P_z^+ \rho), \quad (3)$$

which corresponds to the second column in Table 1. For the lower bound, observe that the GHZ state also strictly resides in the subspace of  $P_x^+ \equiv (\mathbf{1} + X_1 X_2 X_3 X_4)/2$  such that its density matrix takes the form  $|\text{GHZ}\rangle\langle\text{GHZ}| = P_z^+ P_x^+$ . We can then use the union bound from probability theory to upper bound the probabilities of being orthogonal to GHZ, which provides a lower bound to the fidelity (2):

$$F_{\text{GHZ}}(\rho) \geq 1 - \text{tr}(P_z^- \rho) - \text{tr}(P_x^- \rho). \quad (4)$$

The first average corresponds to the fraction of runs where the  $Z$  outcomes disagree and is given by the second column in Table 1. The contribution from the  $XXXX$  generator is given by the third column. For the physical and (error-corrected) logical states  $\rho, \bar{\rho}$ , we hence obtain fidelity bounds of

$$97.8 \pm 0.2\% \leq F_{\text{GHZ}}(\rho) \leq 98.7 \pm 0.2\% \quad (5a)$$

$$99.5 \pm 0.15\% \leq F_{\text{GHZ}}(\bar{\rho}) \leq 99.7 \pm 0.1\%. \quad (5b)$$

The statistical significance between the physical upper bound and the logical lower bound is  $\approx 3.6\sigma$ , assuming statistically independent uncertainties.

*Outlook.*— We have prepared a logical GHZ state on four qubits with a higher fidelity than its physical counterpart. The key ingredient is a quantum LDPC code whose long-range interactions enable (i) a compact encoding of logical qubits and (ii) efficient logical entangling gates via qubit permutations. Having demonstrated

the ability to prepare specific quantum entangled logical states beyond break-even, an immediate near-term experimental goal will be to use our encoding (or others) to demonstrate break-even on larger circuits involving multiple logical qubits, eventually including circuits with non-Clifford gates.

Our work highlights an advantage of using quantum LDPC codes in existing hardware over conventional topological codes like the surface and color codes. Of course, a major feature of the topological codes is that they are equipped with transversal implementations of the Clifford group. A big challenge in the field is to construct nonlocal quantum LDPC codes with hardware-efficient logical gates; some progress using hypergraph product codes has been previously made [48, 49]. We hope that this work stimulates further progress in this direction, especially since it is already known that LDPC codes can significantly reduce the overhead for fault-tolerant quantum computation when functioning just as a memory block [45]. On a separate front, nonlocal codes derived from concatenating quantum Hamming codes also show promise for low-overhead fault tolerance [50, 51]. Since these codes are not LDPC, they require more complicated gadgets for fault tolerance. A worthwhile future direction is to perform a detailed cost-benefit analysis between LDPC and concatenated architectures on different hardware.

*Acknowledgements.*— This work was supported in part by the Alfred P. Sloan Foundation under Grant FG-2020-13795 (AL), by the Air Force Office of Scientific Research under Grant FA9550-24-1-0120 (YH, AL), and by the Office of Naval Research via Grant N00014-23-1-2533 (YH, AL). Additionally, we thank the hardware team at Quantinuum for making these experiments possible.

- 
- [1] A.Yu. Kitaev, “Fault-tolerant quantum computation by anyons,” *Annals of Physics* **303**, 2–30 (2003).
- [2] H. Bombin and M. A. Martin-Delgado, “Topological quantum distillation,” *Phys. Rev. Lett.* **97**, 180501 (2006).
- [3] Eric Dennis, Alexei Kitaev, Andrew Landahl, and John Preskill, “Topological quantum memory,” *Journal of Mathematical Physics* **43**, 4452–4505 (2002).
- [4] Andrew J. Landahl, Jonas T. Anderson, and Patrick R. Rice, “Fault-tolerant quantum computing with color codes,” (2011), [arXiv:1108.5738 \[quant-ph\]](https://arxiv.org/abs/1108.5738).
- [5] Lukas Postler, Sascha Heußen, Ivan Pogorelov, Manuel Rispler, Thomas Feldker, Michael Meth, Christian D. Marciniak, Roman Stricker, Martin Ringbauer, Rainer Blatt, Philipp Schindler, Markus Müller, and Thomas Monz, “Demonstration of fault-tolerant universal quantum gate operations,” *Nature* **605**, 675–680 (2022), [arXiv:2111.12654 \[quant-ph\]](https://arxiv.org/abs/2111.12654).
- [6] C. Ryan-Anderson, J. G. Bohnet, K. Lee, D. Gresh, A. Hankin, J. P. Gaebler, D. Francois, A. Chernoguzov, D. Lucchetti, N. C. Brown, T. M. Gatterman, S. K. Halit, K. Gilmore, J. A. Gerber, B. Neyenhuis, D. Hayes, and R. P. Stutz, “Realization of real-time fault-tolerant quantum error correction,” *Phys. Rev. X* **11**, 041058 (2021).
- [7] Google Quantum AI, “Suppressing quantum errors by scaling a surface code logical qubit,” *Nature* **614**, 676–681 (2023).
- [8] Dolev Bluvstein, Simon J. Evered, Alexandra A. Geim, Sophie H. Li, Hengyun Zhou, Tom Manovitz, Sepehr Ebadi, Madelyn Cain, Marcin Kalinowski, Dominik Hangleiter, J. Pablo Bonilla Ataides, Nishad Maskara, Iris Cong, Xun Gao, Pedro Sales Rodriguez, Thomas Karolyshyn, Giulia Semeghini, Michael J. Gullans, Markus Greiner, Vladan Vuletić, and Mikhail D. Lukin, “Logical quantum processor based on reconfigurable atom arrays,” *Nature* **626**, 58–65 (2023).
- [9] M. P. da Silva, C. Ryan-Anderson, J. M. Bello-Rivas, A. Chernoguzov, J. M. Dreiling, C. Foltz, F. Frachon, J. P. Gaebler, T. M. Gatterman, L. Grans-Samuelsson, D. Hayes, N. Hewitt, J. Johansen, D. Lucchetti, M. Mills,

- S. A. Moses, B. Neyenhuis, A. Paz, J. Pino, P. Siegfried, J. Strabley, A. Sundaram, D. Tom, S. J. Wernli, M. Zanner, R. P. Stutz, and K. M. Svore, “Demonstration of logical qubits and repeated error correction with better-than-physical error rates,” (2024), [arXiv:2404.02280 \[quant-ph\]](#).
- [10] Craig Gidney and Martin Ekerå, “How to factor 2048 bit rsa integers in 8 hours using 20 million noisy qubits,” *Quantum* **5**, 433 (2021).
- [11] Sergey Bravyi, David Poulin, and Barbara Terhal, “Tradeoffs for reliable quantum information storage in 2d systems,” *Phys. Rev. Lett.* **104**, 050503 (2010).
- [12] Nikolas P. Breuckmann and Jens Niklas Eberhardt, “Quantum low-density parity-check codes,” *PRX Quantum* **2** (2021), [10.1103/prxquantum.2.040101](#).
- [13] Jean-Pierre Tillich and Gilles Zemor, “Quantum ldpc codes with positive rate and minimum distance proportional to the square root of the blocklength,” *IEEE Transactions on Information Theory* **60**, 1193–1202 (2014).
- [14] Matthew B. Hastings, Jeongwan Haah, and Ryan O’Donnell, “Fiber bundle codes: Breaking the  $n^{1/2}$  polylog( $n$ ) barrier for quantum ldpc codes,” (2020), [arXiv:2009.03921 \[quant-ph\]](#).
- [15] Pavel Pantelev and Gleb Kalachev, “Quantum ldpc codes with almost linear minimum distance,” *IEEE Transactions on Information Theory* **68**, 213–229 (2022).
- [16] Nikolas P. Breuckmann and Jens N. Eberhardt, “Balanced product quantum codes,” *IEEE Transactions on Information Theory* **67**, 6653–6674 (2021).
- [17] Pavel Pantelev and Gleb Kalachev, “Asymptotically good quantum and locally testable classical ldpc codes,” (2022), [arXiv:2111.03654 \[cs.IT\]](#).
- [18] Irit Dinur, Min-Hsiu Hsieh, Ting-Chun Lin, and Thomas Vidick, “Good quantum ldpc codes with linear time decoders,” (2022), [arXiv:2206.07750 \[quant-ph\]](#).
- [19] Anthony Leverrier and Gilles Zémor, “Quantum tanner codes,” (2022), [arXiv:2202.13641 \[quant-ph\]](#).
- [20] Daniel Gottesman, “Fault-tolerant quantum computation with constant overhead,” (2014), [arXiv:1310.2984 \[quant-ph\]](#).
- [21] Omar Fawzi, Antoine Groppe, and Anthony Leverrier, “Constant overhead quantum fault-tolerance with quantum expander codes,” in *2018 IEEE 59th Annual Symposium on Foundations of Computer Science (FOCS)* (IEEE, 2018).
- [22] Nouédyne Baspin and Anirudh Krishna, “Quantifying nonlocality: How outperforming local quantum codes is expensive,” *Phys. Rev. Lett.* **129**, 050505 (2022).
- [23] Nouédyne Baspin, Omar Fawzi, and Ala Shayeghi, “A lower bound on the overhead of quantum error correction in low dimensions,” (2023), [arXiv:2302.04317 \[quant-ph\]](#).
- [24] Sergey Bravyi, Andrew W. Cross, Jay M. Gambetta, Dmitri Maslov, Patrick Rall, and Theodore J. Yoder, “High-threshold and low-overhead fault-tolerant quantum memory,” *Nature* **627**, 778–782 (2024), [arXiv:2308.07915 \[quant-ph\]](#).
- [25] Qian Xu, J. Pablo Bonilla Ataides, Christopher A. Pattison, Nithin Raveendran, Dolev Bluvstein, Jonathan Wurtz, Bane Vasić, Mikhail D. Lukin, Liang Jiang, and Hengyun Zhou, “Constant-overhead fault-tolerant quantum computation with reconfigurable atom arrays,” *Nature Physics* (2024), [10.1038/s41567-024-02479-z](#).
- [26] Yifan Hong, Matteo Marinelli, Adam M. Kaufman, and Andrew Lucas, “Long-range-enhanced surface codes,” (2024), [arXiv:2309.11719 \[quant-ph\]](#).
- [27] Joshua Viszlai, Willers Yang, Sophia Fuhui Lin, Junyu Liu, Natalia Nottingham, Jonathan M. Baker, and Frederic T. Chong, “Matching Generalized-Bicycle Codes to Neutral Atoms for Low-Overhead Fault-Tolerance,” (2023), [arXiv:2311.16980 \[quant-ph\]](#).
- [28] C. Ryan-Anderson, N. C. Brown, M. S. Allman, B. Arkin, G. Asa-Attuah, C. Baldwin, J. Berg, J. G. Bohnet, S. Braxton, N. Burdick, J. P. Campora, A. Chernoguzov, J. Esposito, B. Evans, D. Francois, J. P. Gaebler, T. M. Gatterman, J. Gerber, K. Gilmore, D. Gresh, A. Hall, A. Hankin, J. Hostetter, D. Lucchetti, K. Mayer, J. Myers, B. Neyenhuis, J. Santiago, J. Sedlacek, T. Skripka, A. Slattery, R. P. Stutz, J. Tait, R. Tobey, G. Vittorini, J. Walker, and D. Hayes, “Implementing fault-tolerant entangling gates on the five-qubit code and the color code,” [arXiv:2208.01863 \(2022\)](#).
- [29] S. A. Moses, C. H. Baldwin, M. S. Allman, R. Ancona, L. Ascarrunz, C. Barnes, J. Bartolotta, B. Bjork, P. Blanchard, M. Bohn, J. G. Bohnet, N. C. Brown, N. Q. Burdick, W. C. Burton, S. L. Campbell, J. P. Campora, C. Carron, J. Chambers, J. W. Chan, Y. H. Chen, A. Chernoguzov, E. Chertkov, J. Colina, J. P. Curtis, R. Daniel, M. DeCross, D. Deen, C. Delaney, J. M. Dreiling, C. T. Ertsgaard, J. Esposito, B. Estey, M. Fabrikant, C. Figgatt, C. Foltz, M. Foss-Feig, D. Francois, J. P. Gaebler, T. M. Gatterman, C. N. Gilbreth, J. Giles, E. Glynn, A. Hall, A. M. Hankin, A. Hansen, D. Hayes, B. Higashi, I. M. Hoffman, B. Horning, J. J. Hout, R. Jacobs, J. Johansen, L. Jones, J. Karcz, T. Klein, P. Lauria, P. Lee, D. Liefer, S. T. Lu, D. Lucchetti, C. Lytle, A. Malm, M. Matheny, B. Mathewson, K. Mayer, D. B. Miller, M. Mills, B. Neyenhuis, L. Nugent, S. Olson, J. Parks, G. N. Price, Z. Price, M. Pugh, A. Ransford, A. P. Reed, C. Roman, M. Rowe, C. Ryan-Anderson, S. Sanders, J. Sedlacek, P. Shevchuk, P. Siegfried, T. Skripka, B. Spaun, R. T. Sprenkle, R. P. Stutz, M. Swallows, R. I. Tobey, A. Tran, T. Tran, E. Vogt, C. Volin, J. Walker, A. M. Zolot, and J. M. Pino, “A race-track trapped-ion quantum processor,” *Phys. Rev. X* **13**, 041052 (2023).
- [30] D. Kielpinski, C. Monroe, and D. J. Wineland, “Architecture for a large-scale ion-trap quantum computer,” *Nature* **417**, 709–711 (2002).
- [31] Jonathan P. Home, David Hanneke, John D. Jost, Jason M. Amini, Dietrich Leibfried, and David J. Wineland, “Complete methods set for scalable ion trap quantum information processing,” *Science* **325**, 1227–1230 (2009), <https://www.science.org/doi/pdf/10.1126/science.1177077>.
- [32] J. M. Pino, J. M. Dreiling, C. Figgatt, J. P. Gaebler, S. A. Moses, M. S. Allman, C. H. Baldwin, M. Foss-Feig, D. Hayes, K. Mayer, C. Ryan-Anderson, and B. Neyenhuis, “Demonstration of the trapped-ion quantum-ccd computer architecture,” *Nature* (2020), [10.1038/s41586-021-03318-4](#), [arXiv:2003.01293 \[quant-ph\]](#).
- [33] V. Kaushal, B. Lekitsch, A. Stahl, J. Hilder, D. Pijn, C. Schmiegelow, A. Bermudez, M. Müller, F. Schmidt-Kaler, and U. Poschinger, “Shuttling-based trapped-ion quantum information processing,” *AVS Quantum Science* **2**, 014101 (2020), [https://pubs.aip.org/avs/aqs/article-pdf/doi/10.1116/1.5126186/19738817/014101\\_1\\_online.pdf](https://pubs.aip.org/avs/aqs/article-pdf/doi/10.1116/1.5126186/19738817/014101_1_online.pdf).
- [34] M Saffman, “Quantum computing with atomic qubits

- and rydberg interactions: progress and challenges,” *Journal of Physics B: Atomic, Molecular and Optical Physics* **49**, 202001 (2016).
- [35] Antoine Browaeys and Thierry Lahaye, “Many-body physics with individually controlled Rydberg atoms,” *Nature Physics* **16**, 132–142 (2020).
- [36] Adam M Kaufman and Kang-Kuen Ni, “Quantum science with optical tweezer arrays of ultracold atoms and molecules,” *Nature Physics* **17**, 1324–1333 (2021).
- [37] Simon J. Evered, Dolev Bluvstein, Marcin Kalinowski, Sepehr Ebadi, Tom Manovitz, Hengyun Zhou, Sophie H. Li, Alexandra A. Geim, Tout T. Wang, Nishad Maskara, Harry Levine, Giulia Semeghini, Markus Greiner, Vladan Vuletić, and Mikhail D. Lukin, “High-fidelity parallel entangling gates on a neutral-atom quantum computer,” *Nature* **622**, 268–272 (2023).
- [38] Daniel Gottesman, “Stabilizer codes and quantum error correction,” (1997), [arXiv:quant-ph/9705052](https://arxiv.org/abs/quant-ph/9705052) [quant-ph].
- [39] A. R. Calderbank and Peter W. Shor, “Good quantum error-correcting codes exist,” *Phys. Rev. A* **54**, 1098–1105 (1996).
- [40] Andrew Steane, “Multiple-particle interference and quantum error correction,” *Proceedings of the Royal Society of London. Series A: Mathematical, Physical and Engineering Sciences* **452**, 2551–2577 (1996).
- [41] Argyris Giannisis Manes and Jahan Claes, “Distance-preserving stabilizer measurements in hypergraph product codes,” (2023), [arXiv:2308.15520](https://arxiv.org/abs/2308.15520) [quant-ph].
- [42] Yu Tomita and Krysta M. Svore, “Low-distance surface codes under realistic quantum noise,” *Phys. Rev. A* **90**, 062320 (2014).
- [43] Joschka Roffe, David R. White, Simon Burton, and Earl Campbell, “Decoding across the quantum low-density parity-check code landscape,” *Phys. Rev. Res.* **2**, 043423 (2020).
- [44] Joschka Roffe, “LDPC: Python tools for low density parity check codes,” (2022).
- [45] Lawrence Z. Cohen, Isaac H. Kim, Stephen D. Bartlett, and Benjamin J. Brown, “Low-overhead fault-tolerant quantum computing using long-range connectivity,” *Science Advances* **8** (2022), [10.1126/sciadv.abn1717](https://doi.org/10.1126/sciadv.abn1717).
- [46] Anders Sørensen and Klaus Mølmer, “Quantum computation with ions in thermal motion,” *Phys. Rev. Lett.* **82**, 1971–1974 (1999).
- [47] Richard Jozsa, “Fidelity for Mixed Quantum States,” *J. Mod. Opt.* **41**, 2315–2323 (1994).
- [48] Anirudh Krishna and David Poulin, “Fault-tolerant gates on hypergraph product codes,” *Phys. Rev. X* **11**, 011023 (2021).
- [49] Armanda O. Quintavalle, Paul Webster, and Michael Vasmer, “Partitioning qubits in hypergraph product codes to implement logical gates,” *Quantum* **7**, 1153 (2023).
- [50] Hayata Yamasaki and Masato Koashi, “Time-efficient constant-space-overhead fault-tolerant quantum computation,” *Nature Physics* **20**, 247–253 (2024).
- [51] Satoshi Yoshida, Shiro Tamiya, and Hayata Yamasaki, “Concatenate codes, save qubits,” (2024), [arXiv:2402.09606](https://arxiv.org/abs/2402.09606) [quant-ph].